Heliyon 10 (2024) e35505

Contents lists available at ScienceDirect

Heliyon

journal homepage: www.cell.com/heliyon

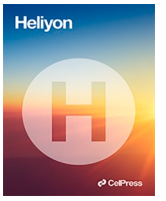

Research article

Nano-catalytic behavior of CeO_2 nanoparticles in dye adsorption: Synthesis through bio-combustion and assessment of UV-light-driven photo-adsorption of indigo carmine dye

Sanjay S. Majani [a], Manoj [a], M. Lavanya [a], B. Swathi [a], N. Anuvarna [a], Muzaffar Iqbal [b], Shiva Prasad Kollur [a,*]

[a] School of Physical Sciences, Amrita Vishwa Vidyapeetham, Mysuru Campus, Mysuru, 570 026, Karnataka, India
[b] Department of Pharmaceutical Chemistry, College of Pharmacy, King Saud University, Riyadh, 11451, Saudi Arabia

ARTICLE INFO

Keywords:
Bio-combusted
Indigo carmine
UV-Light-driven
Manilkara zapota

ABSTRACT

This study explores the adsorption of indigo carmine dye using bio-combusted cerium oxide nanoparticles (CeO_2 NPs). CeO_2 NPs were synthesized using a bio-combustion method, and then subjected to structural, morphological, and optical characterization for thorough investigation. Structural investigation was carried out using X-ray diffraction (XRD), which revealed a cubic structure with evaluated average crystallite size of 11.55 nm. Later, the same was verified by employing W–H plot (13.57 nm). UV–Vis spectroscopy revealed an effective band gap of 3 eV suited for photocatalytic applications. The metal-oxygen phonon band at 986.32 cm^{-1} and 871.96 cm^{-1} is confirmed using Infrared Spectroscopy (FTIR). The morphological analysis was done using Transmission and Scanning Electron Microscopy (TEM and SEM), which revealed well-dispersed, aggregated structure enclosing spherical nanoparticles with an average size of ~14 nm. The early precursors were validated using EDAX analysis and SEM. Optical characteristics were investigated using photoluminescence (PL), which revealed a large charge transfer band between 360 nm and 435 nm. The dye removal efficiency of CeO_2 NPs was evaluated against Indigo Carmine dye using UV light. The results showed that the significantly adsorption, with more than 70 % removed after 150 min. Kinetic experiments revealed that the depreciation occurred via a pseudo-first-order reaction process. Furthermore, the impacts of certain factors such as dye dosage, pH, reusability, and scavenger on adsorption rate were explored and shown to be effective values for the adsorption process. This study emphasizes the potential of CeO_2 NPs as excellent photocatalysts for environmental remediation, especially in dye removal applications.

1. Introduction

During the recent few years, the engineering field of nanotechnology has felt the demand of going green in the synthesis of nanoparticles. This is in response to the demands of reducing negative impact that the traditional way presents to the environment. Among all kinds of nanomaterials, Cerium Oxide nanoparticles (CeO_2 NPs) have been identified as one of the most suitable solutions thanks to their numerous favorable characteristics of their physical-chemical properties, wide application in various branches of

* Corresponding author.
E-mail address: shivachemist@gmail.com (S.P. Kollur).

https://doi.org/10.1016/j.heliyon.2024.e35505
Received 20 June 2024; Received in revised form 22 July 2024; Accepted 30 July 2024
Available online 31 July 2024

science including catalysis, energetics, and medicine [1–3]. The synthesis of CeO_2 NPs using plant extract as a green synthesis procedure has attracted a lot of interest due to its environmentally friendly synthesis process and has the ability to synthesize a large quantity of the nanoparticles [4,5].

As industries continue to expand at a rapid rate, their operations have resulted in the emission of dangerous chemicals into the environment. This has raised serious worries about not just the environment, but also human health [6,7]. In response to the problem, researchers have been motivated to develop long-term remedies (Table 1). One intriguing line of research has been the creation of new materials capable of resolving these important concerns [8]. CeO_2 nanoparticles, well-known for their exceptional catalytic and photocatalytic capabilities [9–11], have emerged as an effective tool in environmental rehabilitation efforts. The green production of these nanoparticles with plant extracts is particularly interesting. This novel strategy takes advantage of phytochemicals' inherent reducing and stabilizing properties, providing a feasible and long-term solution to the situation at hand. Plant extracts are increasingly being used in nanoparticle production due to their high concentration of bioactive components such as polyphenols, flavonoids, and alkaloids [12,13]. Along with acting as reducing and stabilizing agents, these phytochemicals provide unique functional properties to the nanoparticles generated [14]. Using green approaches to produce CeO_2 nanoparticles improves the environment while also providing a cost-effective alternative to typical chemical procedures. Furthermore, the inherent biocompatibility of plant extracts reduces the toxicity risks associated with synthetic chemicals, broadening the prospective uses of these nanoparticles in biomedical and environmental sectors [15].

The use of CeO_2 nanoparticles for photocatalysis has emerged as a key advance since it utilizes energy > band gap energy to break down organic contaminants. The pervasive occurrence of dyes in industrial effluents has brought attention to the need for appropriate remedies due to their tenacious nature and harmful ecological repercussions. CeO_2 nanoparticles' distinctive bandgap structure and adept charge transfer skills have shown to be very efficient in photocatalytic degradation, making them ideal for dealing with organic dye contaminants. Furthermore, the green production approach enhances the attraction of these nanoparticles by encouraging ecologically beneficial actions throughout the entire process [23–25].

Sapodilla, commonly known as chiku or *Manilkara Zapota*, has emerged as a vital resource in nanotechnology due to its significant contributions to green synthesis [26–28]. This tropical fruit, high in bioactive chemicals, provides an environmentally acceptable option for generating a variety of nanoparticles. By introducing *Manilkara Zapota* into the green synthesis process, we not only take advantage of its abundance but also connect with the growing emphasis on sustainable and ecologically friendly approaches in nanomaterial manufacturing. Nanoparticles driven by *Manilkara Zapota* have unique properties that make them ideal for application in photocatalysis and antibacterial activities [29,30]. Through careful synthesis, these nanoparticles have outstanding photocatalytic abilities, making them vital in breaking down contaminants and cleansing water supplies. The use of *Manilkara Zapota* in nanoparticle synthesis not only demonstrates the adaptability of natural resources, but also helps to the development of novel and environmentally friendly technologies with prospective applications in a variety of sectors.

The current work focuses on the photocatalytic effectiveness of bio-combusted CeO_2 NPs using *Manilkara Zapota* L. extract. The prepared sample was analyzed for phase identification, optical characteristics, size, and form. Furthermore, its efficacy in adsorbing Indigo Carmine (IC) dye was examined, and studies was extended to investigate the kinetics of adsorption.

2. Experimental

2.1. Materials and methods

The *Manilkara zapota* plant leaves were acquired from the Manasagangothri campus of University of Mysore, Mysuru, Karnataka, India, in the month of October. Sigma (USA) supplied the precursor, cerium nitrate hydrate ($Ce(NO_3)_3.6H_2O$). The phase of the as-prepared samples was determined using a MALVERN PANALYTIC X'pert^3. In addition, the morphology of the surface and elemental content of the samples were evaluated using the ZEISS FESEM. The excellently resolved JOEL JEM-2100 plus TEM was used to determine the average particle size with more precision. To explore the band gap and perform photocatalysis, a UV-3200 Lab India A double beam UV–visible spectrophotometer was used. Finally, the SHIMADZU IR, Xross over was used to record the FTIR spectrum.

Table 1
Biomaterial comparison in remediate pollutants.

Sl. No.	Material	Green resources	Pollutant	Reference
1	Ag NPs	*Saussurea costus* Root extract	Methylene Blue, Phenol red, Methyl Orange, Orange G, Congo Red, and Safranin O	[16]
2	ZrO_2 NPs	*water hyacinth* plant extract	Methyl Orange and Methylene Blue	[17]
3	Ag-doped CuO NPs	*Heracleum persicum* Extract	Erythrosine and Rhodamine B	[18]
4	FeNPs	*Vernonia Amygdalina* leaf extract	Crystal Violet and Methylene Blue.	[19]
5	TiO_2 NPs	*Rosmarinus-officinalis* leaf extract	Methylene Blue	[20]
6	–	*water hyacinth*	Cd(II) and Pb(II) ions	[21]
7	–	*Ziziphus spina-christi*	Pb(II), Zn(II) and Cd(II) ions	[22]

2.2. Preparation of Manilkara zapota L. Extract

Manilkara zapota plant leaves were properly cleansed with double distilled water and placed in a 250 mL beaker with 100 mL water. The mixture was heated for an extended period of time until 100 mL was reduced to 25 mL of leaf extract (L. extract). The combination was then filtered, and the filtrate was stored at 4 °C for further characterization.

2.3. Bio-synthesis of CeO_2 NPs employing Manilkara zapota L. Extract

A bio-mediated solution combustion synthesis (SCS) was employed in fabricating CeO_2 NPs. Initially, 3.26 g of $Ce(NO_3)_3.6H_2O$ was weighed stoichiometrically and taken in a combustion vessel (ceramic crucible). Into that, 5 ml of freshly prepared *Manilkara zapota* L. extract was added as a fuel along with double distilled water and allowed to stir for 30 min in order to obtain the homogeneous mixture. The same was then introduced into a pre-heated muffle furnace operated at 500 °C, where a normal combustion reaction occurs, giving pale-yellow colored amorphous results. Furthermore, the obtained product was calcined for 2 h at 750 °C to obtained the desired CeO_2 NPs. The same was subjected to characterize further for phase identification, size, shape, and optical properties. Furthermore, the same method was utilized to chemically synthesize CeO_2 NPs.

2.4. Adsorption of IC dye using CeO_2 nanocatalyst

The ability of chemically and bio-synthesized CeO_2 to adsorb IC dye reactants was investigated in an uv chamber that contained a magnetic stirrer. An amiciVision (AV-31-UV) LED torch produced homogeneous UV light from all sides. The photocatalytic tests involve creating four separate 5 ppm dye solutions and evaluating their adsorption against various photocatalyst dosages of 5 mg, 10 mg, 15 mg, and 20 mg. Before the adsorption began, the separate solutions containing 5 ppm dye and the appropriate concentration of photocatalyst were swirled in darkness for 60 min to achieve adsorption-desorption equilibrium. Every 30 min, 3 mL of the stock solution was withdrawn and centrifuged to measure absorbance using UV–visible spectroscopy until the dye was fully adsorbed. The recovered catalyst was again utilized in evaluating the reusability. Furthermore, the same was studied vice-versa, 20 mg photocatalyst was used to degrade dye solution of different concentration like, 5, 10, 15, and 20 ppm. Later, both the adsorption mechanism was evaluated on calculating adsorption capacity (%D) using the relation (1),

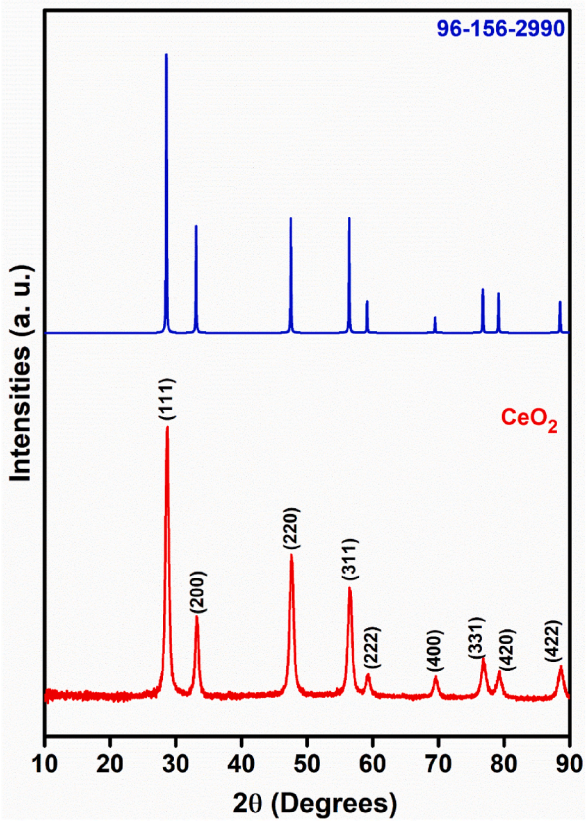

Fig. 1. PXRD profile of CeO_2 NPs well in agreement with the card #96-156-2990.

$$\%D = \left(\frac{A_0 - A_t}{A_0}\right) \times 100 \quad (1)$$

3. Results and discussions

3.1. Phase identification studies

X-Ray Diffraction (XRD) analysis plays a critical role in studying the phase and structural information of nanomaterials, making it a vital tool in various applications. The fabricated CeO_2 NPs were also subjected to PXRD analysis for structural information. Fig. 1 shows the PXRD pattern well in alignment with the JCPDS card #96-156-2990, having a cubic phase with Fm-3m space group. The structural parameters were found as, $\alpha = \beta = \gamma = 90^\circ$ with $a = b = c = 5.4070$ Å. Crystal planes at $2\theta = 28.76^\circ$, 33.21°, 47.60°, 56.44°, 59.16°, 69.53°, 76.85°, 79.29°, and 88.67 were assigned to (111), (200), (220), (311), (222), (400), (331), (420), and (422), respectively. The same were utilized in evaluating the averaged crystallite size utilizing the relation 2 (Scherrer's relation) [31].

$$D_{hkl} = \frac{0.9 * \lambda}{\beta_{hkl} \cos\theta} \quad (2)$$

wherein, D_{hkl}; crystallite size, β_{hkl}; Full Width at Half Maximum (FWHM) of the diffraction peaks obtained, θ; diffracting angle, and λ; wavelength of the X-Rays used. 0.9 being the shape factor for spherical nanoparticles on approximating the fabricated CeO_2 NPs to be spherical in shape. The evaluated average crystallite size was found to be 11.55 nm. The same was verified on plotting the Williamson-Hall (W–H) relation (3) [32] for the corresponding diffraction peaks as shown in Fig. 2. The obtained value was well in correspondence with the evaluated crystallite size (13.57 nm) with a strain component (ε) value of 1.2×10^{-3} and R^2 value of 0.9678.

$$\beta_{hkl} \cos\theta = 4\varepsilon \sin\theta + \frac{0.9\lambda}{D_{hkl}} \quad (3)$$

3.2. Band gap studies

The ability to absorb photons for photocatalytic activities of the as-prepared CeO_2 NPs, the as-prepared sample is investigated using UV–visible spectra (Fig. 3a). The UV peak reflectance band (400 and 600 nm) is attributed to the exchange of charge between Ce^{3+} and O^{2-}. The same was utilized in evaluating the band gap value using Kubelka-Munk function (4) [33],

$$F(R_\infty) = \frac{(1 - R_\infty)^2}{2R_\infty} \quad (4)$$

$$h\nu = \frac{1240}{\lambda} \quad (5)$$

R_∞ is depicted as reflectance co-efficient and λ as wavelength of the UV source. The value was found to meet at exact 3.00 eV (Fig. 3b), which can be aligned with the previously reported work [34].

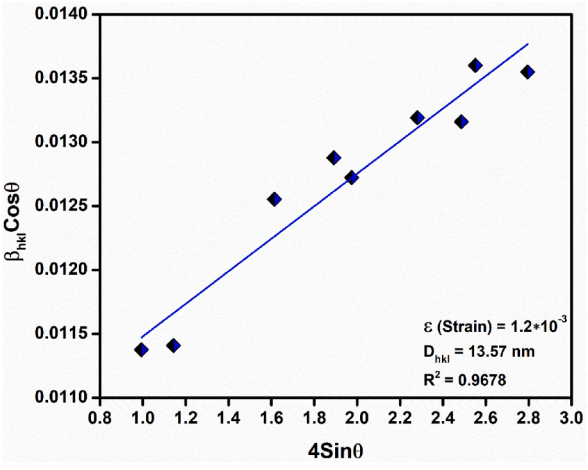

Fig. 2. W–H plot of CeO_2 NPs using the respective diffraction peaks.

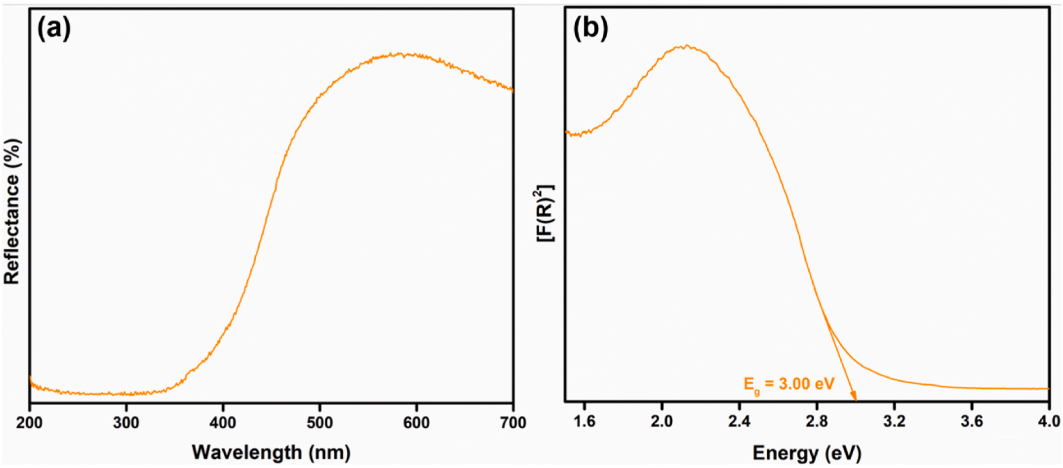

Fig. 3. (a) DRS spectrum of as-synthesized CeO_2 NPs recorded between 200 and 700 nm and (b) respective band-gap evaluation.

3.3. Infrared studies

Fig. 4 depicts the IR spectra of the as-prepared CeO_2 NPs. The spectral band observed at 3710.98 cm^{-1} corresponds to the stretching of O–H bonds, whereas the bands observed at 2286.12 cm^{-1} correspond to the stretching of C–H bonds [35]. Furthermore, the O–H bending band was observed at 1457.18 cm^{-1}. The sample's bands at 986.32 cm^{-1} and 871.96 cm^{-1} might indicate a metal-oxygen phonon interaction (<1000 cm^{-1}) (Ce–O) [36].

3.4. Morphology and purity studies

As nanomaterials reach the nanoscale, their surface morphology dynamically alters, resulting in a continual modulation of their notable properties [37]. The so-fabricated CeO_2 NPs were subjected to morphological studies to know their shape and size. Fig. 5 depicts the FESEM images of CeO_2 NPs, showing agglomerated irregular structure at different magnifications like 2 μm and 1 μm. furthermore, the initial precursors utilized in the synthesis process were confirmed on subjecting the sample to EDAX analysis (Fig. 6).

To have some knowledge about insight morphology, the as-prepared CeO2 NPs were subjected to TEM analysis at different magnification as shown in Fig. 7a (500 nm), 7b (200 nm), and 7c (50 nm). the observed results affirm the morphology of crystal cluster enclosing nanospheres. The average particle size was calculated to be ~14 nm using ImageJ software which was in well agreement with the PXRD data. Further, to align the crystal structure obtain from PXRD analysis SAED image was taken and the crystal planes (111), (220), and (311) were identified as marked in Fig. 7d. Also, to evaluate the lattice spacing of the obtained crystal array, HRTEM image (Fig. 7e and f) was recorded and analyzed for selected area using ImageJ software. The spacing between crystal array was found to be 0.311 nm.

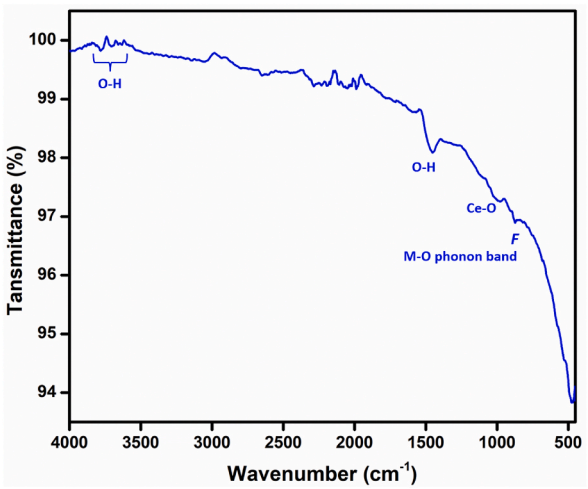

Fig. 4. IR spectrum confirming the metal-complex formation in as-prepared CeO_2 NPs.

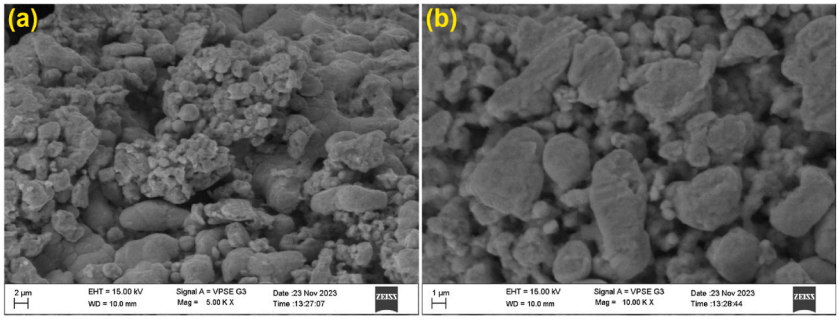

Fig. 5. SEM images of prepared CeO_2 NPs at (a) 2 µm and (b) 1 µm magnification.

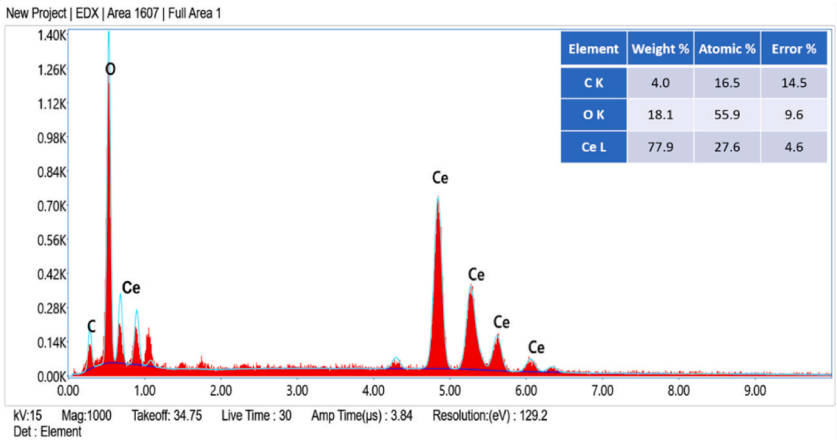

Fig. 6. EDAX spectrum affirming the precursors used in the synthesis process.

3.5. Emission spectrum

The emission spectrum is one of the most useful tools in the evaluation of dye removal process as it offers extensive information. Accordingly, the emission spectrum of as-prepared CeO_2 NPs was recorded between 300 and 500 nm at 240 nm excitation (Fig. 8), showing the characteristic CeO_2 band from 360 nm to 435 nm owning to the effective charge transfer band (CTB). Particularly, the $Ce^{4+}/4f$ electron transfer process to the O 2p band will have a greater role in cerium-based photocatalysts. This band helps in improving the photocatalytic activity by allowing the flow of electrons in an effective manner to degrade the dye on exposure to light source [38].

3.6. *Nanocatalyst dosage effect*

Dye removal treatment by using the photocatalytic technique is described as follows: indicated photocatalyst CeO_2 NPs in four different concentrations of (5 mg, 10 mg, 15 mg and 20 mg) were dispersed all through four solutions of 5 ppm of Indigo Carmine (IC) dye. These solutions were ultrasonically agitated for 60 min in the dark to achieve adsorption-desorption equilibrium of the photocatalyst/dye system. These were done by exposing the solutions to UV light while the solutions were being stirred immediately after the adsorption and desorption equilibrium periods. At every 30-min interval, 3 mL of the stock solutions was taken. The photocatalyst was removed from the treated solution through centrifugation, further, the UV–vis spectrum was recorded at each interval using a spectrophotometer. The procedure was continued until there was no further adsorption of IC dye was observed.

The UV–visible absorption spectra of IC dye with photocatalyst dosage exposed to UV light for various time are presented in Fig. 9a-d. The absorption peaks at 610 nm [39] for IC dye adsorption demonstrate that as the exposure of sunlight on solution rises the intensity of peaks declines proving the adsorption of IC dye in presence of UV light. This is due to the acquired electrostatic attraction between positively charged photocatalyst and negatively charged IC dye molecule [40,41]. The adsorption process might also be possible due to the hydrogen bonding, π- π interactions, and hydrophobic interactions between the IC dye molecule and photocatalyst [42].

Furthermore, the effective CeO_2 NPs dosage to deal a considerable amount of IC dye adsorption was found to be 20 mg, after careful evaluation of %D depicted in Fig. 9e-h later the same was authenticated by performing kinetics involved in the respective adsorption part using 1st order kinetic relation (7) [43].

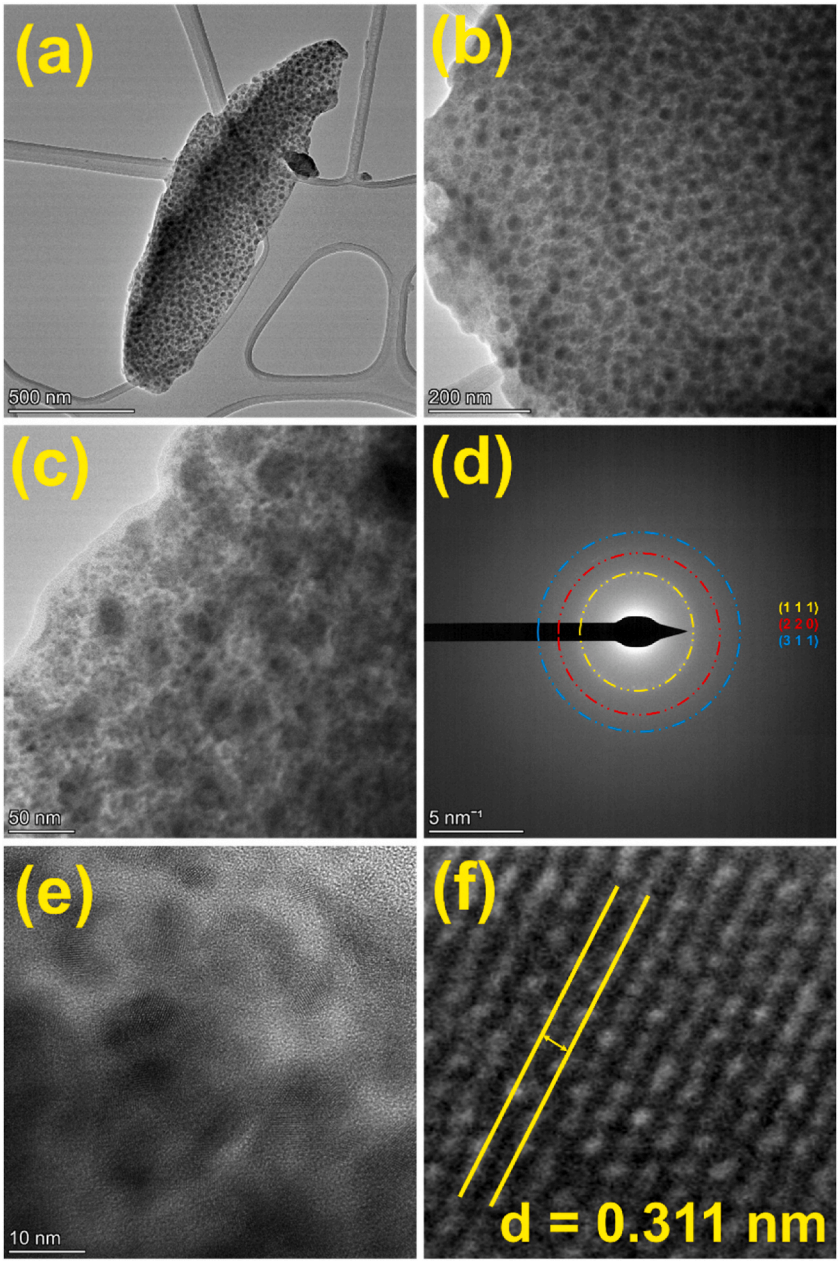

Fig. 7. TEM images (a–c), SAED image (d), and d-spacing evaluation (e and f) of as-synthesized CeO_2 NPs.

$$\log\left(A_0/A\right) = kt \tag{7}$$

where; A_0 being the absorbance at respective 0 min and A being the absorbance at respective times. Adsorption kinetics of 5 ppm IC dye against 20 mg photocatalyst was found to be best with k value of 0.00359 and R^2 of 0.976. The results of photocatalyst dosage effect are briefed in Table 2.

3.7. Dye dosage, reusability, pH, and scavenger effect on %D

It is necessary to investigate how parameters including dye dosage, pH, reusability, and the nature of scavenger impacts the capability of adsorbing dye efficiently and sustainably. They are determining factors of the rate of degradation, cost, and ecological effect of the treatment, thus providing adequate removal of detrimental dyes from the effluents [44]. The dye removal efficacy of the

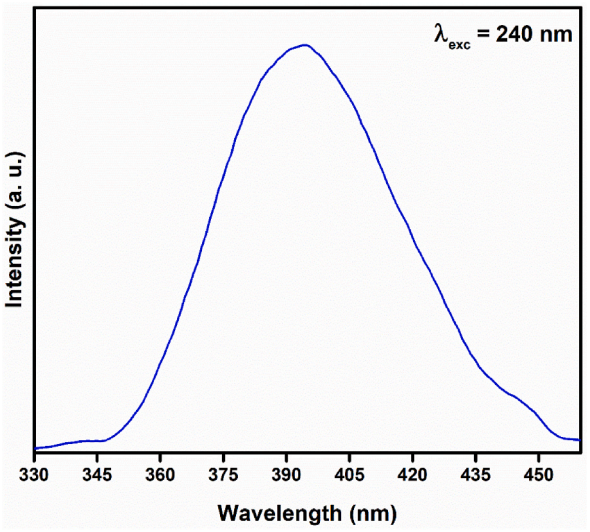

Fig. 8. Emission spectrum of as-prepared CeO_2 NPs.

20 mg CeO_2 NPs sample towards different IC dye concentrations is displayed in Fig. 10a. At starting concentrations of 5, 10, 15, and 20 ppm, respectively, the adsorption efficiencies were 70.62 %, 22.30 %, 21.66 %, and 13.48 %. A 150-min reaction time and the number of CR molecules still present were used to calculate the adsorption efficiency. The adsorption efficiency decreasing as the initial concentration of CR increases indicating the system's oxidation and reduction processes to be constrained by a fixed number of radical species. Therefore, the longer it takes for the solution to totally decompose, the more IC dye molecules there are in it.

The effect of pH on dye adsorption is critical due to its substantial impact on the efficiency and pace of dye removal and the overall environmental and treatment results. Hence, the pH effect was investigated by changing the pH of the dye solution from 1 to 11. The result indicates the pH 4 is suitable in adsorbing IC dye to 73.21 % (Fig. 10b). Further, the photocatalyst, CeO_2 NPs were recovered after the adsorption process to conduct reusability test. Fig. 10c depicts the same with a small decrement in the adsorption rate after the 4th usage showing the stability of the prepared sample.

Scavenger studies were performed to determine the species of reactive oxygen that are accountable for the photo-catalytic breakdown of IC dyes. Minute quantities of scavenging species, such as *p*-benzoquinone (BQ), ethylenediaminetetraacetic acid (EDTA), and isopropyl alcohol (IP) have been introduced to neutralize the reactive oxygen compounds (ROS) such as hydroxyl radical $^{\bullet}OH$, superoxide radical $^{\bullet}O^{2-}$, and hole h^{+}, generated during photocatalysis [45,46]. Fig. 10d depicts the dye removal activity of CeO_2 NPs with respective scavengers introduced. Hydroxyl radicals ($^{\bullet}OH$) do not play a major role in the dye removal process, as indicated by the fact that the medium's adsorption efficiency did not decrease upon the addition of IP. However, adding BQ and EDTA during the process resulted in a significant reduction in adsorption efficiency. The drop in efficiency indicates that the species of reactive oxygen (ROS) produced mostly react with the scavengers. This finding suggests that superoxide radicals ($^{\bullet}O^{2-}$) and holes (h^{+}) play a role in the photocatalytic activity of CeO_2 NPs during photocatalysis. A detail representation of IC dye adsorption is shown in Fig. 11. Furthermore, the chemically synthesized CeO_2 NPs were utilized in degrading the same IC dye with same catalyst (20 mg) and dye dosage (10 ppm). The results show a comparatively low adsorption rate (~19 %) as depicted in Fig. S1 against the bio-synthesized CeO_2 NPs. This result affirms that the bio-synthesized CeO2 NPs is more advantages over chemically synthesized CeO_2 NPs in degrading IC dye.

4. Conclusion

In conclusion, this study reveals the efficient adsorption of indigo carmine dye utilizing bio combusted cerium oxide nanoparticles (CeO_2 NPs). A bio-combustion approach was successfully employed to synthesize the CeO_2 NPs, and the synthesized sample was subjected to extensive structural, morphological, and optical characterization. The cubic structure of the nanoparticles was verified by XRD and the W–H plot, with crystallite sizes of around 11.55 nm and 13.57 nm, respectively. A suitable band gap of 3 eV was detected by UV–Vis spectroscopy for photocatalytic applications, and the presence of typical metal-oxygen phonon bands at 986.32 cm^{-1} and 871.96 cm^{-1} was confirmed by FTIR. The early precursors were subsequently validated by EDAX analysis, which also showed well-dispersed clusters surrounding spherical nanoparticles with an average size of around 14 nm. PL investigation revealed a large charge transfer band between 360 and 435 nm, which improved the photocatalytic activities of CeO_2 NPs. The photocatalyst dosage effect was examined first when evaluating the photocatalytic efficacy against the dye indigo carmine. The 20 mg dose had the most noteworthy performance among the four photocatalyst dosages—5 mg, 10 mg, 15 mg, and 20 mg—against the 5-ppm dye solution, reaching over 70 % adsorption in 150 min under UV light. A pseudo-first-order reaction mechanism was followed by the adsorption kinetics. Furthermore, the parameter analysis demonstrated the influence of dye concentration (efficient at 5 ppm), pH (efficient at value 4 with 73.21 %), reusability, and scavengers on the adsorption rate, all contributing to the efficient adsorption process. The findings suggest that CeO_2 NPs synthesized through bio-combustion can offer a sustainable and efficient approach in addressing

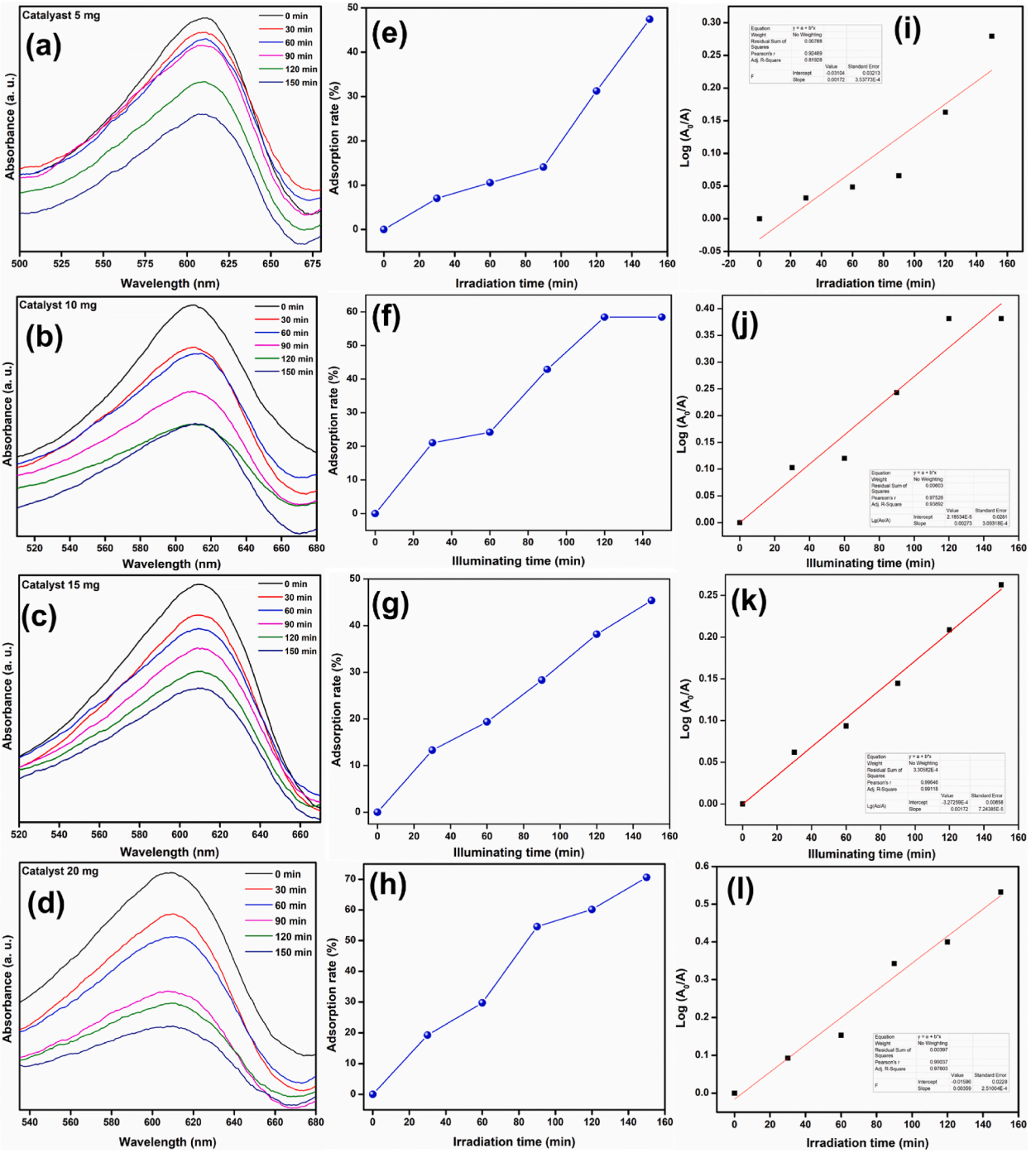

Fig. 9. (a–d) Time-dependent CeO_2 photocatalyst dosage effect on the absorbance spectra of IC dye, following (e–h) %D at respective time and (i–l) kinetics involved in respective adsorption.

environmental pollution caused by industrial dyes.

CRediT authorship contribution statement

Sanjay S. Majani: Writing – original draft, Methodology, Investigation, Formal analysis, Data curation, Conceptualization. **Manoj:** Resources, Investigation. **M. Lavanya:** Investigation, Formal analysis. **B. Swathi:** Formal analysis, Data curation. **N. Anuvarna:** Methodology, Investigation. **Muzaffar Iqbal:** Visualization, Validation, Software. **Shiva Prasad Kollur:** Writing – review & editing,

Table 2
Results of photocatalyst dosage effect on 5 ppm IC dye solution.

Photocatalyst Dosage (mg)	%D	Kinetics	
		k value	R^2
5	47.42	0.00172	0.813
10	58.44	0.00273	0.938
15	45.37	0.00172	0.991
20	70.62	0.00359	0.976

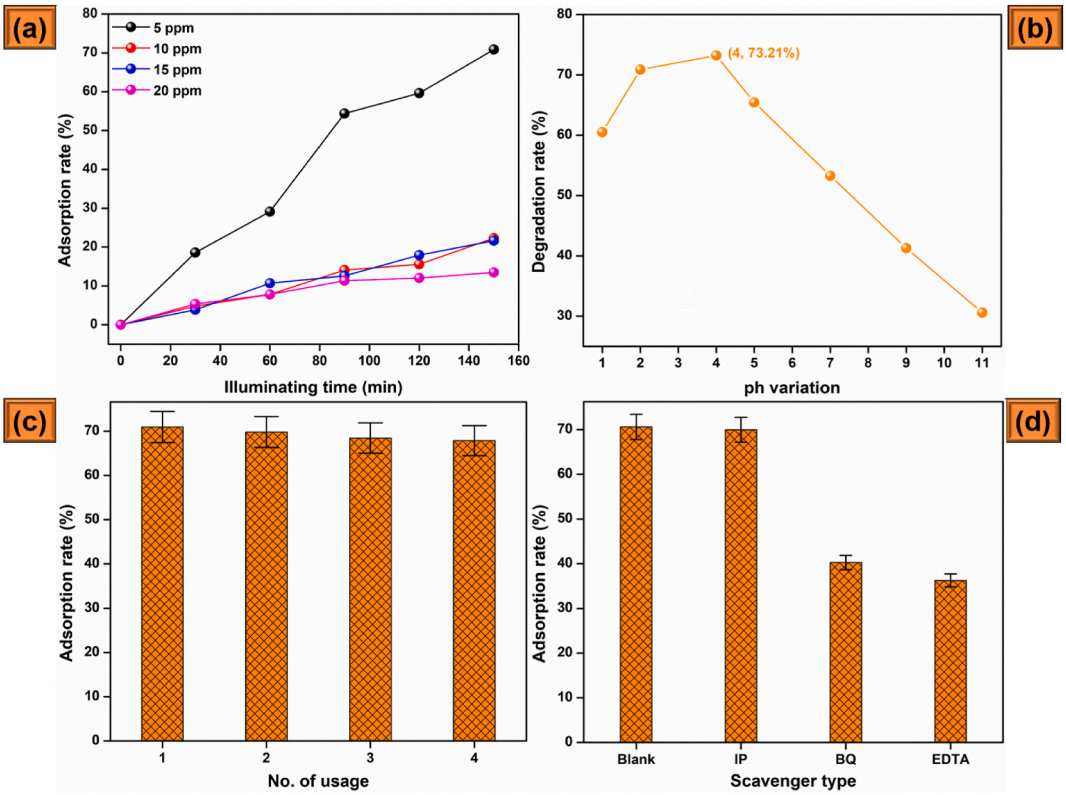

Fig. 10. Effect of (a) Dye dosage, (b) pH, (c) reusability, and (d) scavenger type on adsorption rate of IC dye.

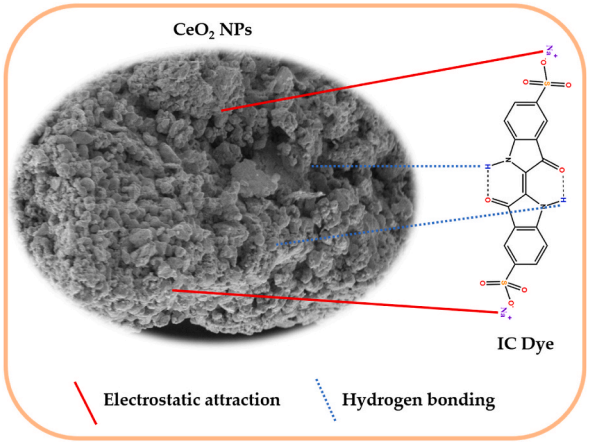

Fig. 11. Detailed representation of IC dye adsorption on bio-synthesized CeO_2 NPs.

Visualization, Supervision, Project administration.

Declaration of competing interest

The authors declare that they have no known competing financial interests or personal relationships that could have appeared to influence the work reported in this paper.

Acknowledgements

Authors thank the director of Amrita Vishwa Vidyapeetham, Mysuru campus for providing instrumentation and infrastructure facilities. The authors extend their appreciation to Researchers Supporting Project number (RSPD2024R734), King Saud University, Riyadh, Saudi Arabia.

Appendix A. Supplementary data

Supplementary data to this article can be found online at https://doi.org/10.1016/j.heliyon.2024.e35505.

References

[1] S. Ge, J. Zhang, H. Xiao, C. Du, Y. Jin, J. Yao, C. Zhang, Ni nanoparticles supported on CeO_2 as catalysts for aqueous-phase glycerol reforming, ACS Appl. Nano Mater. 7 (10) (2024) 11498–11505, https://doi.org/10.1021/acsanm.4c01101.
[2] X.-M. Cao, J.-Q. Chen, X.-R. Zhao, H. Ge, D. Liu, Q. Wu, Z.-J. Sun, Q. Zhang, Facile synthesis of bead-chain structured MWCNTs@CeO_2 with oxygen vacancies-rich for promoting electrochemical energy storage, Chem. Eng. J. 479 (2024) 147663, https://doi.org/10.1016/j.cej.2023.147663.
[3] V. Sarnatskaya, Y. Shlapa, D. Kolesnik, O. Lykhova, D. Klymchuk, S. Solopan, S. Lyubchyk, I. Golovynska, J. Qu, Y. Stepanov, A. Belous, Bioactivity of cerium dioxide nanoparticles as a function of size and surface features, Biomater. Sci. 12 (10) (2024) 2689–2704, https://doi.org/10.1039/D3BM01900D.
[4] N. Korkmaz, D. Kısa, Y. Ceylan, E. Güçlü, F. Şen, A. Karadağ, Synthesis of CeO_2 nanoparticles from hemp leaf Extract: evaluation of Antibacterial, anticancer and enzymatic activities, Inorg. Chem. Commun. 159 (2024) 111797, https://doi.org/10.1016/j.inoche.2023.111797.
[5] S.J.S. Al Khafaji, M. Ghobeh, M. Mashergi, A. Es-haghi, Biological synthesis of cerium oxide nanoparticles using funnel extract: characterization and evaluation of its angiogenesis and cytotoxicity properties against breast cancer cells, BioNanoScience (2024), https://doi.org/10.1007/s12668-024-01355-7.
[6] S. Dutta, S. Adhikary, S. Bhattacharya, D. Roy, S. Chatterjee, A. Chakraborty, D. Banerjee, A. Ganguly, S. Nanda, P. Rajak, Contamination of textile dyes in aquatic environment: adverse impacts on aquatic ecosystem and human health, and its management using bioremediation, J. Environ. Manag. 353 (2024) 120103, https://doi.org/10.1016/j.jenvman.2024.120103.
[7] D.K. Anusha, A study on -role of textile industry in environment pollution: a case study, EPRA International Journal of Multidisciplinary Research (IJMR) 10 (1) (2024) 202–207. https://eprajournals.net/index.php/IJMR/article/view/3565.
[8] Z.M. Şenol, N. El Messaoudi, Z. Ciğeroglu, Y. Miyah, H. Arslanoğlu, N. Bağlam, E.S. Kazan-Kaya, P. Kaur, J. Georgin, Removal of food dyes using biological materials via adsorption: a review, Food Chem. 450 (2024) 139398, https://doi.org/10.1016/j.foodchem.2024.139398.
[9] J.M. Soney, T. Dhannia, Enhanced photocatalytic activity of CeO_2 and magnetic biochar-CeO_2 nanocomposite prepared from Murraya koenigii stem for degradation of methyl orange under UV light, J. Photochem. Photobiol. Chem. 447 (2024) 115259, https://doi.org/10.1016/j.jphotochem.2023.115259.
[10] Z. Cheng, X. Wang, T. Li, S. Gao, D. Gao, Q. Guo, L. Wang, X. Hu, Facile synthesis of nano CeO_2/sepiolite composite as visible-light-driven photocatalyst for rapid tetracycline removal, J. Environ. Chem. Eng. 12 (3) (2024) 112829, https://doi.org/10.1016/j.jece.2024.112829.
[11] K. Vanasundari, P. Ponnarasi, G. Mahalakshmi, A green approach to synthesis of Ag-doped CeO_2 nanorods embedded reduced graphene oxide nanocomposite for excellent photocatalytic and antimicrobial activity, Inorg. Chem. Commun. 165 (2024) 112523, https://doi.org/10.1016/j.inoche.2024.112523.
[12] S. Bhatt, S. Saraswat, A review on phytochemical mediated synthesis of nanoparticles through fruits and vegetables extract and their potential applications, Nanotechnology for Environmental Engineering (2024), https://doi.org/10.1007/s41204-024-00370-z.
[13] C. Jayaseelan, P. Upadhyay, D. Sahal, C. Kamaraj, R. Thirugnanasambandam, D. Siva, D. Saravanan, R. Regina Mary, Biosynthesis of gold nanoparticles mediated by medicinal phytometabolites: an effective tool against Plasmodium falciparum and human breast cancer cells, J. Drug Deliv. Sci. Technol. 95 (2024) 105520, https://doi.org/10.1016/j.jddst.2024.105520.
[14] G. Rana, P. Dhiman, A. Kumar, S. Selvaraj, A. Chauhan, G. Sharma, Phytomediated synthesis of Fe_3O_4 nanoparticles using Cannabis sativa root extract: photocatalytic activity and antibacterial efficacy, Biomass Conversion and Biorefinery (2024), https://doi.org/10.1007/s13399-024-05785-x.
[15] N. Alarfaj, N. Al Musayeib, M. Amina, M. El-Tohamy, Synthesis and characterization of polysiphonia/cerium oxide/nickel oxide nanocomposites for the removal of toxins from contaminated water and antibacterial potential, Environ. Sci. Pollut. Control Ser. 31 (11) (2024) 17064–17096, https://doi.org/10.1007/s11356-024-32199-z.
[16] B.U. Hijazi, M. Faraj, R. Mhanna, M.H. El-Dakdouki, Biosynthesis of silver nanoparticles as a reliable alternative for the catalytic degradation of organic dyes and antibacterial applications, Current Research in Green and Sustainable Chemistry 8 (2024) 100408, https://doi.org/10.1016/j.crgsc.2024.100408.
[17] S. Pandey, J. Chaudhary, H. Sharma, S. Pundir, S. Rustagi, S. Malik, P. Choudhary, Biosynthesis of zirconia nanoparticles (ZrO_2) by water hyacinth: characterization and its photocatalytic dye degradation activity, Biomass Conversion and Biorefinery (2024), https://doi.org/10.1007/s13399-024-05529-x.
[18] R.A. Ghazi, A.S. Jasim, K. Heydaryan, H. Khojasteh, M. Mohammadalizadeh, S.A. Kadhim, V. Eskandari, Biosynthesis of Ag-doped CuO nanoparticles using heracleum persicum extract for enhanced antibacterial and photocatalytic dye degradation properties, Plasmonics (2024), https://doi.org/10.1007/s11468-024-02298-1.
[19] Y.S. Jara, T.T. Mekiso, A.P. Washe, Highly efficient catalytic degradation of organic dyes using iron nanoparticles synthesized with Vernonia Amygdalina leaf extract, Sci. Rep. 14 (1) (2024) 6997, https://doi.org/10.1038/s41598-024-57554-5.
[20] A. Saka, L.T. Jule, B. Badassa, L. Gudata, N. Nagaprasad, R. Shanmugam, L.P. Dwarampudi, V. Seenivasan, K. Ramaswamy, Biosynthesis of TiO_2 nano particles by using Rosemary (Rosmarinus officinalis) leaf extracts and its application for crystal dye degradation under sunlight, BMC Chemistry 18 (1) (2024) 123, https://doi.org/10.1186/s13065-024-01229-9.
[21] H.S. Ibrahim, N.S. Ammar, M. Soylak, M. Ibrahim, Removal of Cd(II) and Pb(II) from aqueous solution using dried water hyacinth as a biosorbent, Spectrochim. Acta Mol. Biomol. Spectrosc. 96 (2012) 413–420, https://doi.org/10.1016/j.saa.2012.05.039.
[22] E.A. Assirey, S.M. Sirry, H.A. Burkani, M.A. Ibrahim, Modified Ziziphus spina-christi stones as green route for the removal of heavy metals, Sci. Rep. 10 (1) (2020) 20557, https://doi.org/10.1038/s41598-020-76810-y.
[23] A. Bhardwaj, A.K. Singh, Biogenic synthesis, characterization and photocatalytic activity of cerium nanoparticles for treatment of dyes contaminated water, Biocatal. Agric. Biotechnol. 57 (2024) 103075, https://doi.org/10.1016/j.bcab.2024.103075.

[24] Zeng, S., Shui, A., Yu, H., & He, C. Sonochemical synthesis of CeO2 nanoparticles with high photocatalytic and antibacterial activities under visible light. Int. J. Appl. Ceram. Technol. https://doi.org/https://doi.org/10.1111/ijac.14775.
[25] M. Mylarappa, S. Chandruvasan, K.S. Harisha, R. Sandhya, K.N. Shravana Kumara, S.G. Prasanna Kumar, H. Madival, Green synthesis of natural gomutra and honey doped CeO_2 nanocomposite for green sensor, cyclic voltammetry, photocatalysis and antioxidant studies, Green Technologies and Sustainability 2 (2) (2024) 100085, https://doi.org/10.1016/j.grets.2024.100085.
[26] R.J. Naik, P.A. Kumar, G. Alekhya, Y. Subbareddy, G.R. Kandregula, S. Mandal, Fabrication of high voltage and energy dense supercapacitor with Manilkara zapota seeds derived porous activated carbon in acidic electrolyte, Inorg. Chem. Commun. 164 (2024) 112365, https://doi.org/10.1016/j.inoche.2024.112365.
[27] P. Muthumari, J. Dhanalakshmi, M. Petchimuthu, M. Jeeva, R.M. Akash, S. Naveen, S. Madhu, Synthesis of iron nanoparticles by aqueous extract of Manilkara zapota leaves and evaluation of the antimicrobial activity, AIP Conf. Proc. 3170 (1) (2024), https://doi.org/10.1063/5.0215797.
[28] P. Sharma, A. Deep, H. Kumar, N. Bansal, S. Kumar, Arun, D. Kumar, Pharmacological potential of (L.) P. Royen (Sapodilla): a narrative review, J. Tradit. Chin. Med. 44 (2) (2024) 403–407, https://doi.org/10.19852/j.cnki.jtcm.2024.02.001.
[29] R.M. Kiriyanthan, S.A. Sharmili, R. Balaji, S. Jayashree, S. Mahboob, K.A. Al-Ghanim, F. Al-Misned, Z. Ahmed, M. Govindarajan, B. Vaseeharan, Photocatalytic, antiproliferative and antimicrobial properties of copper nanoparticles synthesized using Manilkara zapota leaf extract: a photodynamic approach, Photodiagnosis Photodyn. Ther. 32 (2020) 102058, https://doi.org/10.1016/j.pdpdt.2020.102058.
[30] D. Ayodhya, A. Ambala, G. Balraj, M. Pradeep Kumar, P. Shyam, Green synthesis of CeO_2 NPs using Manilkara zapota fruit peel extract for photocatalytic treatment of pollutants, antimicrobial, and antidiabetic activities, Results in Chemistry 4 (2022) 100441, https://doi.org/10.1016/j.rechem.2022.100441.
[31] S.S. Majani, R.B. Basavaraj, K.N. Venkatachalaiah, T. Chandrasekhar, S.P. Kollur, Versatile deep red-emitting $SrCeO_3$: Eu^{3+} nanopowders for display devices and advanced forensic applications, J. Solid State Chem. 329 (2024) 124360, https://doi.org/10.1016/j.jssc.2023.124360.
[32] K. Patel, A. Patel, V.P. Jethwa, H. Patel, G.K. Solanki, X-ray diffraction analysis of orthorhombic SnSe nanoparticles by Williamson–Hall, Halder–Wagner and Size–Strain plot methods, Chemical Physics Impact 8 (2024) 100547, https://doi.org/10.1016/j.chphi.2024.100547.
[33] P.R. Jubu, O.S. Obaseki, D.I. Ajayi, E. Danladi, K.M. Chahrour, A. Muhammad, S. Landi, T. Igbawua, H.F. Chahul, F.K. Yam, Considerations about the determination of optical bandgap from diffuse reflectance spectroscopy using the tauc plot, J. Opt. (2024), https://doi.org/10.1007/s12596-024-01741-0.
[34] L.D. Sonawane, A.S. Mandawade, L.N. Bhoye, H.I. Ahemad, S.S. Tayade, Y.B. Aher, A.B. Gite, L.K. Nikam, S.D. Shinde, G.H. Jain, G.E. Patil, M.S. Shinde, Sol-gel and hydrothermal synthesis of CeO2 NPs: their physiochemical properties and applications for gas sensor with photocatalytic activities, Inorg. Chem. Commun. 164 (2024) 112313, https://doi.org/10.1016/j.inoche.2024.112313.
[35] M.M. Latif, A.-u. Haq, F. Amin, M. Ajaz-un-Nabi, I.-u. Khan, N. Sabir, Synthesis and antimicrobial activities of Manganese (Mn) and iron (Fe) co-doped Cerium dioxide (CeO_2), Nanoparticles. Physica B: Condensed Matter 600 (2021) 412562, https://doi.org/10.1016/j.physb.2020.412562.
[36] K. Hadjiivanov, Chapter two - identification and characterization of surface hydroxyl groups by infrared spectroscopy, in: F.C. Jentoft (Ed.), Adv. Catal. 57 (2014) 99–318, https://doi.org/10.1016/B978-0-12-800127-1.00002-3. Academic Press.
[37] T. Gholami, H. Seifi, E.A. Dawi, M. Pirsaheb, S. Seifi, A.M. Aljeboree, A.-H.M. Hamoody, U.S. Altimari, M. Ahmed Abass, M. Salavati-Niasari, A review on investigating the effect of solvent on the synthesis, morphology, shape and size of nanostructures, Mater. Sci. Eng., B 304 (2024) 117370, https://doi.org/10.1016/j.mseb.2024.117370.
[38] C. K, S. S.V, J. V.P, V. B A, N. K.M, Photometric study on excitation tailored cyan to white color conversion in $SrCeO_3$: Dy^{3+} for wLEDs, latent fingerprint, and security ink applications, Mater. Today Commun. 38 (2024) 107954, https://doi.org/10.1016/j.mtcomm.2023.107954.
[39] K. Karthik, Keerthi, N. Bernaurdshaw, Box–Behnken Design and experimental studies on novel fibrous g-C_3N_4 towards water splitting and degradation of indigo carmine dye, Int. J. Hydrogen Energy 57 (2024) 939–948, https://doi.org/10.1016/j.ijhydene.2024.01.088.
[40] K.D. Alanazi, B.H. Alshammari, O.A.S. Ahmad, M.M. Aljohani, H.H. Alsharief, A.H. Al-Bagawi, A.H. Alsehli, N.M. El-Metwaly, Citric acid-cross linked with magnetic metal-organic framework composite sponge for superior adsorption of indigo carmine blue dye from aqueous solutions: characterization and adsorption optimization via Box–Behnken design, J. Mol. Struct. 1299 (2024) 137131, https://doi.org/10.1016/j.molstruc.2023.137131.
[41] G. Dabhade, A. Malpure, A. Borhade, Y. Shewale, S. Kushare, G. Daware, Y. Rajesh, Optical CuAl2O4 used as photocatalyst for IC dye degradation, Water Pract. Technol. 19 (5) (2024) 2032–2044, https://doi.org/10.2166/wpt.2024.107.
[42] M.A. Ben Aissa, M. Khairy, M.E. Khalifa, E.A. Abdelrahman, N. Raza, E.M. Masoud, A. Modwi, Facile synthesis of TiO2@ZnO nanoparticles for enhanced removal of methyl orange and indigo carmine dyes: adsorption, kinetics, Heliyon 10 (10) (2024) e31351, https://doi.org/10.1016/j.heliyon.2024.e31351.
[43] N.M. Mahmoodi, M. Arami, N.Y. Limaee, N.S. Tabrizi, Kinetics of heterogeneous photocatalytic degradation of reactive dyes in an immobilized TiO_2 photocatalytic reactor, J. Colloid Interface Sci. 295 (1) (2006) 159–164, https://doi.org/10.1016/j.jcis.2005.08.007.
[44] K.M. Reza, A.S.W. Kurny, F. Gulshan, Parameters affecting the photocatalytic degradation of dyes using TiO_2: a review, Appl. Water Sci. 7 (4) (2017) 1569–1578, https://doi.org/10.1007/s13201-015-0367-y.
[45] M. Zhang, X. Zhao, Y. Dong, C. Hu, X. Xiang, X. Zeng, J. Jia, C. Jin, L. Ding, X. Chen, In-situ synthesis of 0D/1D $CeO_2/Zn_{0.4}Cd_{0.6}S$ S-scheme heterostructures for boosting photocatalytic remove of antibiotic and chromium, Ceram. Int. 49 (4) (2023) 5842–5853, https://doi.org/10.1016/j.ceramint.2022.11.256.
[46] G. Singh, M. Sharma, R. Vaish, Flexible Ag@$LiNbO_3$/PVDF composite film for piezocatalytic dye/pharmaceutical degradation and bacterial disinfection, ACS Appl. Mater. Interfaces 13 (19) (2021) 22914–22925, https://doi.org/10.1021/acsami.1c01314.